 doi:10.20944/preprints202004.0084.v1

In silico Repositioning for Dual Inhibitor Discovery of SARS-CoV-2 (COVID-19) 3C-like Protease and Papain-like Peptidase

Kowsar Bagherzadeh [a,b,*], Kourosh Daneshvarnejad [c], Mohammad Abbasinazari [d], Homa Azizian [e,*]

[a] Eye Research Center, The Five Senses Institute, Rassoul Akram Hospital, Iran University of Medical Sciences, Tehran, Iran

[b] Microbial Biotechnology Research Center, Iran University of Medical Sciences, Tehran, Iran

[c] Department of Medicinal Chemistry, Faculty of Pharmacy, Tehran Medical Sciences, Tehran, Iran

[d] Department of Clinical Pharmacy, School of pharmacy, Shahid Beheshti University of Medical Sciences, Tehran, Iran

[e] Department of Medicinal Chemistry, School of Pharmacy International Campus, Iran University of Medical Sciences, Tehran, Iran

*Correspondence to:

Dr. Homa Azizian, Pharm.D, Ph.D

Department of Medicinal Chemistry, School of Pharmacy, International campus, Iran University of Medical Sciences

Address: Kazem Besarati St., Kabiri Tameh Ave., Shahid Hemmat Expy, International Campus, Tehran, Iran.

Phone: +989122196554

ORCID: 0000-0003-0827-3727

E-mail: azizian.h@iums.ac.ir, homazizian@gmail.com

 doi:10.20944/preprints202004.0084.v1

*Co-correspondence to:

Dr. Kowsar Bagherzadeh, Ph.D

Eye Research Center, The Five Senses Institute, Rassoul Akram Hospital, Iran University of Medical Sciences, Tehran, Iran

Microbial Biotechnology Research Center, Iran University of Medical Sciences, Tehran, Iran

Address: Iran University of Medical Sciences, Shahid Hemmat Highway, Tehran, Iran

Phone: +989126845480

ORCID: 0000-0002-5677-0616

Email: bagherzadeh.k@iums.ac.ir

Abstract

Aims: In late December 2019, early reports predicted the onset of a potential Coronavirus outbreak in china, given the estimate of a reproduction number for the 2019 Novel Coronavirus (COVID-19). Because of high ability of transmission and widespread prevalence, the mortality of COVID-19 infection is growing fast worldwide. Absent of an anti-COVID-19 has put scientists on the urge to repurpose already approved therapeutics or to find new active compounds against coronavirus. Here in this study, a set of computational approaches were performed in order to repurpose antivirals for dual inhibition of the frontier proteases involved in virus replication, papain-like protease (PLpro; corresponding to nsp3) and a main protease (Mpro), 3C-like protease (3CLpro; corresponding to nsp5).

Materials and Methods: In this regard, a rational virtual screening procedure including exhaustive docking techniques was performed for a database of 160 antiviral agents over 3CLpro and PLpro active sites of SARS-CoV-2. The

 doi:10.20944/preprints202004.0084.v1

compounds binding energies and interaction modes over 3CLpro and PLpro active sites were analyzed and ranked with the aid of free Gibbs binding energy. The most potent compounds, based on our filtering process, are then proposed as dual inhibitors of SARSC-CoV-2 proteases.

Key findings: Accordingly, seven antiviral agents including two FDA approved (Nelfinavir, Valaganciclovir) and five investigational compounds (Merimepodib, Inarigivir, Remdesivir, Taribavirine and TAS106-106) are proposed as potential dual inhibitors of the enzymes necessary for RNA replication in which Remdesivir as well as Inagrivir have the highest binding affinity for both of the active sites.

Significance: The mentioned drug proposed to inhibit both PLpro and 3CLpro enzymes with the aim of finding dual inhibitors of SARSC-CoV-2 proteases.

Keywords: in *silico* repositioning; dual inhibitor; Covid-19; 3CLpro; PLpro; remdesivir

1. Introduction

Severe acute respiratory syndrome (SARS) first emerged in Southern China and Hong Kong in 2002, caused by a novel coronavirus (CoV), infecting nearly 8000 people with a mortality rate of over 10% (1). In 2012, Middle East respiratory syndrome coronavirus (MERS-CoV) outspread from Saudi Arabia and infected around 1401 people worldwide with a fatality rate of 39% up to 2015 (2). Although the possibility of highly infectious SARS-like diseases reemergence has remained, there is no approved anti-SARS vaccines and drugs available. Once again, in the last months of 2019 a new coronavirus (SARS-CoV-2 or COVID-19) with fatal viral pneumonia has diagnosed.

 doi:10.20944/preprints202004.0084.v1

Several studies are being performed or on the go to find efficient therapeutics to treat SARS-CoV-2. China's National Health Commission has recommended using HIV-1 protease inhibitors, lopinavir, and ritonavir as an ad hoc treatment against the infection (3). Wang et al. have tested seven FAD-approved drugs against a clinical isolate SARS-CoV-2 and have suggested the assessment of remdesivir and chloroquine for patients suffering from coronavirus disease (4). In addition, the fast progressing researches on epidemiology, genome sequencing, key protein extractions and crystallographic structures generation on SARS-COV-2, is widening our insights into the new coronavirus virus function day by day (5-7).

Coronavirus virus is an enveloped positive-sense single-stranded RNA that eventually cause systemic changes and damage in many vital organs (8). Similar to all viruses, two-thirds of the viral RNA is translated into two large polyproteins which are cleaved by two proteases, Papain-like protease (PLpro) and 3C-like protease (3CLpro) (8, 9). 3CLpro cleave the viral polyproteins to generate the key proteins required for viral maturation (10, 11), replication and the helicase, such as the RNA-dependent RNA polymerase. SARS-CoV-2 3CLpro first crystal structure is recently released (7) and it shows that 3CLpro active pocket is identical to those of other CoVs which means antivirals bind this site can affect wide range of other similar types. PLpro cleaves the two polyproteins to generate the necessary proteins for the virus to replicate. Besides, PLpro has an additional role of stripping ubiquitin to help CoVs evade the host innate immune responses (12, 13). 3CLpro and PLpro has no closely related homologues in humans which makes it an attractive molecular target to design anti-SARS drugs (14).

Daily increasing number of individuals infected by SARS-CoV-2 worldwide and death rate has raised the urge for rapid, concise, and precise strategies to investigate large database of compounds for a certain treatment.

Preprints (www.preprints.org) | NOT PEER-REVIEWED | Posted: 7 April 2020 doi:10.20944/preprints202004.0084.v1

In this study, a set of computational approaches were performed in order to discover repurpose antiviral for dual inhibition of the virus replication procedure. In this regard, a rational virtual screening procedure including exhaustive docking techniques performed over a database of 160 antiviral agents according to Drugbank (15). Compound binding energy and interaction modes over 3CLpro and PLpro active sites were analyzed and ranked. The most potent compounds, based on our filtering process, were then proposed as dual inhibitor of SARSC-CoV-2 protease.

2. Method and Material

2.1 Papain-Like Protease Homology Modeling

Since no crystal structure has been reported for SARS-CoV-2 PLpro yet, SWISS-MODEl workspace (https://swissmodel.expasy.org/interactive) was employed for SARS-CoV-2 PLpro homology modeling (16). PL protease protein sequence was obtained from NCBI GenBank (NCBI Reference Sequence: NC_045512.2), and the homology modeling was performed based on SARS-CoV PLpro crystal structure (PDB:3E9S) as the template with 82.80% sequence similar to the correspondence SARS-CoV-2 PLpro. The quality and validity of the created model was assessed based on Global Model Quality Estimation (GMQE) and QMean.

2.1 Target preparation

In order to monitor the interaction modes of the target molecules over 3CL protease and PLpro enzymes, the Maestro Molecular Modeling platform (version 11.5) by Schrödinger, LLC was used (17). First, the recently released crystal structures of 3CL protease enzyme retrieved from the Protein Data Bank (PDB: 5R82) (http://www.rcsb.org) and the PLpro enzyme structure was obtained by homology modeling.

Preprints (www.preprints.org) | NOT PEER-REVIEWED | Posted: 7 April 2020 doi:10.20944/preprints202004.0084.v1

Except the one structural water molecule in 3CLpro active site, which bridge the receptor important residues by way of H-bonds (His41, Asp187 and His164), the rest of the water molecules were removed from the enzyme crystallographic structure. The Protein Preparation Wizard (18) module was used to prepare the structure of both enzyme properly. Protein Preparation Wizard consists of a set of procedure including; adding the hydrogen atoms, updating and filling the missing side chains residues, respectively, optimizing hydrogen bonds, removing atomic clashes, adding formal charges to the hetero groups and then optimizing at neutral pH. Finally, the structures were minimized using optimized potential for liquid simulations (OPLS3) force field.

The Glide receptor grids constructed based on the co-crystalized ligand-binding sites in the Glide application (Glide, version) of Maestro. The center of each grid was arranged at the centroid of the crystalized ligand-binding site which is set with inner (acceptable space for the ligand center) and outer (search space surrounded all the ligand atoms) box sizes of 10 and 20 Å, respectively. In the case of 3CLpro the hydroxyl group of active site residues of Thr25, Thr45, Ser46, Thr54 and Ser144 are treated as flexible and for PLpro Ser915, Ser990, Ser1009, Tyr1013, Tyr1018 and Tyr1046 were set to rotatable during the docking experiment.

2.2 Database preparation

Total of 160 antiviral agents including; FDA, experimental and investigational agents were collected from Drugbank (15). In order to enrich the database by previously discovered agents known for inhibition of coronavirus 3CLpro, four screened non-peptidic small molecule inhibitors of SARS-CoV 3CLpro were also added to the database. These four compounds were discovered against human SARS-CoV 3CLpro by combination of virtual screening (VS) and high-throughput screening (HTS) of ZINC database, NIH Molecular Libraries and Asinex Platinum

Preprints (www.preprints.org) | NOT PEER-REVIEWED | Posted: 7 April 2020 doi:10.20944/preprints202004.0084.v1

collection (19-21). The LigPrep (22) module were used to prepare ligand structure properly.

2.3 virtual screening workflow

The Virtual Screening Workflow in Maestro was used to dock and score the lead-like compounds to identify potential ligands (23). In order to increase the computational complexity, molecular docking was applied at three different levels of Glide docking precision. During these stages the protocol changes to more rigorous incorporating exhaustive conformational sampling which is a critical requirement for the final stages of the screening. The applied docking level consist of; High Throughput Virtual Screening (HTVS), Standard Precision (SP) and Extra Precision (XP) followed by post processing using Prime molecular mechanics /generalized born surface area (MM-GBSA). During all stages of molecular docking full flexibility was assumed for the ligands. In the HTVS step, up to 10 poses were generated for each compound state and 80% of the best states were preserved and entered the next docking step. During SP step, up to 5 poses were generated and all good scoring states were retained. Screening by the XP docking protocol was performed over 40% of the good states of the SP step. In this step, up to 3 poses were generated for each compound state, and only the best scoring states were kept. Finally, 20% of the best scoring states from the XP docking were generated followed by post-processing using Prime (MM-GBSA) mode to calculate protein-ligand free Gibbs binding energies.

2.4 Prime MM-GBSA

The binding energies (ΔG_{Bind}) were calculated for each compound using Molecular mechanics/generalized born surface area (MM-GBSA) modules (Schrödinger LLC 2018) (24) based on the following equation;

Preprints (www.preprints.org) | NOT PEER-REVIEWED | Posted: 7 April 2020 doi:10.20944/preprints202004.0084.v1

$$\Delta G_{Bind} = E_{Complex} - [E_{Receptor} + E_{Ligand}]$$

where ΔG_{Bind} is the calculated relative free energy which includes both ligand and receptor strain energy. $E_{Complex}$ is the MM-GBSA energy of the minimized complex, and E_{Ligand} is the MM-GBSA energy of the ligand after removing it from the complex and allowing it to relax. $E_{Receptor}$ is the MM-GBSA energy of relaxed protein after separating it from the ligand. The MM-GBSA calculation was performed based on the best pose structure obtained from XP docking complexes.

3. Results and discussion

3.1. Homology modeling of SARS-CoV-2 PLpro

SARS-CoV-2 PLpro homology model was created based on the SARS-CoV PLpro crystal structure (PDB ID: 3E9S), according to the protein sequence obtained from GenBank (Figure1).

Global Model Quality Estimation (GMQE) and QMean are two statistical parameters indicating the validity of the homology models. GMQE is a quality estimation parameter, which encompasses a set of the target-template alignment properties. The GMQE score is a value between 0 and 1 in which higher values indicate higher accuracy and reliability of the model. QMean is a composite estimator of the model quality according to various geometrical properties and reflects both global and local absolute quality estimates based on one single model and shows the quality of the model in comparison with experimental structures. A QMean score near zero shows a higher agreement between the created model and experimental structures that have a similar size (16, 25). This model had a GMQE

Preprints (www.preprints.org) | NOT PEER-REVIEWED | Posted: 7 April 2020 doi:10.20944/preprints202004.0084.v1

score of 0.95 and a QMean score of -0.22, which indicates the high quality of the created model. Besides, the QMean scoring function consists of a linear combination of four individual structural descriptors.

The local quality plot (Figure 2) shows the expected similarity between each residue of the model and the native structure, and the comparison plot (Figure 3) shows the relationship between quality scores of individual models and experimental structures scores with similar size (26). The co-crystallized ligand in 3E9S PDB entry also matched and superimposed with the created model.

3.2. Active site identification enzymes

3.2.1. Active site of 3CLpro

All coronavirus 3CLpro structures are consist of two chymotrypsin-like β-domains; domain I (residues 1-99) and domain II (100-185), and one α-helical dimerization domain III (residues 201-303) and a long loop (residues 185–200) connects domains II and III. The active site is located in the center of the cleft between domains I and II, including a catalytic dyad consisting of His41 and Cys145 (11). The enzyme active site is composed of six subsites (S1-S6). Figure 4a represents the active site cleft along with the residues and the related subsites. S1-subsite is the most important subsite, because is conserved in all coronaviruses. It located at domain I (colored in light green) consists of residues 140–145 and 163–166, which formed the “outer wall” of the S1 site. The S2-subsite, which reside at the interface of domain I and the long loop connecting domain II and III (colored in orange) is formed of Val186, Asp187, Arg188, and Gln189 as well as side-chain atoms of His41, Met49, and

Preprints (www.preprints.org) | NOT PEER-REVIEWED | Posted: 7 April 2020 doi:10.20944/preprints202004.0084.v1

Met165. Residues186–188 line the S2-subsite with some of their main-chain atoms. The S3 side chain is oriented toward bulk solvent. Residues Met165, Leu167, Gln189, Thr190, and Gln192 surround the S4-subsite, which is surrounded at the interface of domain I and II (colored in cyan). The S5-subsite is composed of main-chain atoms of Thr190, Ala191, and Gln192 and S6 sub-site is almost at the outer area of the enzyme (11, 27).

3.2.2. Active site of PLpro

The PLpro monomer is consists of 4 domains including the extended ubiquitin-like domain (UBL), the thumb domain, the palm domain and the fingers domain (12). The active site is located at the interface of the thumb and palm sub-domains and contains a classic catalytic triad, composed of Cys856–His1017–Asp1031, adjacent to the flexible BL2 loop containing Trp851 (according to the homology modeled structure residue numbering). The enzyme has four substrate recognition subsites (S1-S4) (26). Figure 4b represents the active site, the residues and the related subsites. S1 and S2-subsites are mostly buried. S1-subsite includes residues Gly1016, Trp851, Cys856, and Tyr857. Residues Leu907, Asp909, Gly1016, and Tyr1018 are involved in shaping the conserved S2-subsite (residues colored in orange). S3-subsite is partially solvent-exposed and include Gly2016. Like S1 and S2, S4 is also buried and is structured by Asp1047, Pro993, Tyr1009, Tyr1013, Tyr1018, and Thr1046 (residues colored in purple) (28). S2 and S4-subsites are the binding sites for SARS-CoV PLpro competitive inhibitors (28, 29).

3.3. Reliability of docking protocol

The applied docking procedure reliability was validated by re-docking of RZs and TTT over 3CL protease (5R82) and the homology model of PLpro SARS-CoV-2,

Preprints (www.preprints.org) | NOT PEER-REVIEWED | Posted: 7 April 2020 doi:10.20944/preprints202004.0084.v1

respectively. The docked conformations corresponding to the lowest glide score were selected as the most possible binding modes. The root mean square deviation (RMSD) was calculated for ligands to measure the docking prediction accuracy. The pose was counted optimal if its RMSD found to be less than 2 Å. The RMSD of the re-docked conformations of RZs and TTT over 3CLpro and PLpro were 0.40 Å and 0.45, respectively, which is in acceptable value and considered as successfully docked (30, 31). As a result, the validity of Glide dock parameters are reasonable in order to predict the related co-crystalized structures.

Docking of the co-crystalized ligand (RZs) over 3CL protease active site showed that the ring center of the pyridyl moiety interacted the binding pocket by establishing T-shape π-π interaction with Tyr41. In addition, the 4-amide group of the pyridine ring interacts by H-bond interaction with the side chain carbonyl group of Gln186 (C=O) (1.81 Å) (Figure 5a). Furthermore, docking of TTT over PLpro showed the prominent role of Asp909 and Tyr1013 in stabilizing the ligand in the binding pocket by constructing H-bond and π-π stacking interactions with the amide (-NH) and aromatic rings of compound, respectively (Figure 5b).

3.4. Virtual ligand screening of antiviral agents over protease targets of SARS-CoV-2

A structure-based virtual screening was performed following the computational complexity (three different levels of Glide docking precision) protocol of virtual screening workflow module in maestro (Schrödinger) over the recently released 3CLpro SARS-CoV-2 crystallographic structure and the homology model of PLpro, to screen potential small-molecule compounds from the constructed antiviral database (160 compounds). Reliability of the Glide docking procedure was validated by re-docking the co-crystallized ligand over the correspondence crystal structure. Free Gibbs energy (Kcal/mol) based on MM-GBSA method used to score Glide

Preprints (www.preprints.org) | NOT PEER-REVIEWED | Posted: 7 April 2020 doi:10.20944/preprints202004.0084.v1

docking results. Compounds with lower calculated free Gibbs energy (Kcal/mol) are considered to have higher binding affinities with the target protein.

3.4.1. Investigating screening compounds over 3CLpro active site

By performing the virtual screening workflow, a set of 22 compounds was elucidated with considerable binding affinity in value ranges of -69.96 to -25.49 over the 3CLpro active site (Table 1).

Figures 6 and 7 represent chemical structures of the resulted compounds in which twelve of the best score compounds are known FDA antivirals (Indinavir, Tenofovir alafenamide, Valganciclovir, Amprenavir, Boceprevir, Sofosbuvir, Asunaprevir, Darunavir, Atazanavir, Nelfinavir and Ritonavir) and the rest are under investigation agent (Inarigivir, Adafosbuvir, Remdesivir, Merimepodib, L-756423, Taribavirin, TAS-106, Galidesivir, Sorivudine) (Table 2).

According to the obtained results shows on Table 1, Inarigivir, Telaprivir, Indinavir, Adafosbuvine, Tenofouvire, Remdesivir, Valagancyclovir and amprenavir are the compounds with the highest free binding energy (higher than -50 kcal/mol) over 3CLpro active site.

Table 1 also shows the residue interactions of the best score compounds which indicated all compounds fit well into the active site binding pocket and stabilized by forming H-bond interaction with indicated residues belongs to the domain I (residues 2-99), II (residues 100-182) and a long loop between residues 185-200 (11). Furthermore, it reveals the role of His41 residue for interacting the most of the compounds through forming H-bond and hydrophobic π-π stacking interaction.

According to the table 2, antiviral activity of Inarigrivir in combination with Tenofovir (an inhibitor of viral polymerase and anti-HIV agent) is under clinical investigation for Chronic Hepatitis B infection in adults. Telaprevir is a NS3/4a

Preprints (www.preprints.org) | NOT PEER-REVIEWED | Posted: 7 April 2020 doi:10.20944/preprints202004.0084.v1

protease inhibitor, which is used to treat chronic HCV genotype 1 infection. Telaprevir is interacting through hydrogen bond formation with Ser46 and Gln182 main chain amines as well as Glu166 α-carboxyl group. Indinavir, another HIV viral protease enzyme used to treat HIV, has a Glid score close to that of Taleprevir while its free Gibbs energy is considerably higher than Taleprevir. Indinavir receive two hydrogen bonds from Asn142 and Gly143 as well as interacts the binding pocket through hydrogen bond formation as well as π-π stacking and electrostatic interactions with His41 and Glu166, respectively (Table 1).

Adafosbuvir is an under investigation compound for chronic hepatitis C virus (HCV) infection treatment also give a considerable affinity for 3CLpro catalytic site. The compound form hydrogen bonds with Gly143 and Gln189 main chain amines and form π-π stacking interactions with His41. Remdesivir, given a good free Gibbs binding energy, is a nucleoside analog which inhibits the action of RNA virus polymerase (Table 2) through attaching into RNA, blocking the addition of nucleotides and finally terminating the RNA transcription (32). Valganciclovir and Amprenavir are the two other FDA approved antivirals with almost equivalent free Gibbs energy (Lower than -50 Kcal/mol) for 3CLpro which are inhibitors of viral DNA polymerases and HIV viral proteinase enzyme, respectively. Finally, Boceprevir, Sofosbuvir, Asunaprevir, Darunavir, Atazanavir, Nelfinavir, and Ritonavir are other FDA approved compounds that have been extracted from the constructed database (with free Gibbs energy≤ -35) which are mainly applied to treat human immunodeficiency (HIV) virus and chronic hepatitis C (HCV) virus infections.

3.4.2. Investigating screening compounds over PLpro active site

 doi:10.20944/preprints202004.0084.v1

The virtual screening workflow was also performed over PLpro active site and a set of 22 compounds was elucidated with considerable affinity and the structure of the ones solely inhibit PLpro are shown in Figures 7 and 8.

Table 3 shows the binding energy scores along with the residue interaction of the best score compounds over the SARS-CoV-2 PLpro active site. According to the obtained results for PLpro, Elsulfavirine has the highest affinity for PLpro with a free Glide docking score of -76.13 Kcal/mol. Elsulfavirine interacts with PLpro substrate binding site by H-bond formation with Asp909, Gln1014 and Tyr1018 as well as hydrophobic and electrostatic interactions with Tyr1013 and Lys902, respectively. The compound antiviral activity is under investigation for hepatic impairment (Table 2).

Merimepodib is another investigational compound with an inhibition activity against inosine monophospate dehydrogenase, to be used to treat hepatitis C virus and other RNA/DNA viruses infection (Table2). Lopinavir, an approved inhibitor of HIV-1 protease enzyme, is also an antiviral already proposed for its probable anti-SARS-CoV-2 activity (33, 34), and here it presents a considerable affinity for PLpro. It interacts the active site through hydrogen bond formation with Arg911 and hydrophobic interaction with Tyr 1013. The forth compound in the row is Maribavir, an investigations compound for use/treatment in viral infection, that interacts with Asp909, Gln1014, Tyr1018, and Tyr1013 through H-bond formation and hydrophobic interactions. Faldaprevir is an investigational compound to treat chronic hepatitis C (HCV) and intercalate with the active site mainly by hydrogen bond formation with residues Asp909, Arg911, Glu912 and Tyr1013. Inarigivir and Remdesivir both establish interactions with almost similar free Gibss binding energies. Nelfinavir and Valaganciclovir also interact with PLpro with close free Gibss binding energies and Glide docking scores. GS-6620, Penciclovir, Vidarabine,

Preprints (www.preprints.org) | NOT PEER-REVIEWED | Posted: 7 April 2020 doi:10.20944/preprints202004.0084.v1

Taribavirin, Cytarabine, 5-Guanylylmethylenebisphosphonate, TAS-106, Acorbic-acid, 2-deoxyglucose, Ribavirin, and Zanamivir are other FDA Approved/Investigational compounds that have been extracted from the constructed database (with free Gibbs energies between -44 to -19 Kcal/mol) which are applied to treat severe respiratory syncytial virus infection, Influenza A and B infection, chronic hepatitis C (HCV) virus infections, and Herpes simplex infection (Table 2).

3.4.3. *in silico* study of proposed dual inhibitor over SARS-CoV-2 3CLpro and PLpro active site

The identical structures over the two active sites including; Nelfinavir, Valaganciclovir, Merimepodib, Inarigivir, Remdesivir, Taribavirine and TAS106 exist in both screening results based on considerable binding affinities for both target protease enzymes (Tables 1, 2 and 3 compounds highlighted in yellow color). Figures 7 represent chemical structures of the proposed dual inhibitors in which Valganciclovir and Nelfinavir are known FDA antivirals and the rest are under investigation agent (Inarigivir, Remdesivir, Merimepodib, Taribavirin, TAS-106) (Table 2)

Figure 9 depicts the binding interaction of these compounds over 3CLpro. All compounds interact to the shallow substrate-binding site at the surface of each domains I and II.

Inarigrivir with the highest affinity for 3CLpro stabilized in the active pocket mainly through H-bond formation with backbone of Gly143, Ser144 at top of the S1-subsite cavity (Figure 9a). The thiouridylyl moiety oriented toward S2 and S4-subsites through H-bond formation with the backbone of His41(C=O) and Gln189 side chain. These binding interactions probably disturb Cys145-His41 catalytic dyad that mediate protease activity (11) by targeting the thiophosphate moiety in front of

Preprints (www.preprints.org) | NOT PEER-REVIEWED | Posted: 7 April 2020 doi:10.20944/preprints202004.0084.v1

catalytic Cys145 which may provide nucleophilic attack of the catalytic Cys145 onto the thiophosphate group of the inhibitor.

In the case of Remdesivir, it interacts to the S1-subsite through H-bond interaction of propionate and hydroxyl ribose groups with the backbone of Gly143 and the side chain of Glu166, respectively (Figure 9b). In addition, the phenoxy and adenine part of the compound inserted deeply to the S2 and S4-subsites through T-shape π-π and H-bond interaction with His41 and Thr190 (C=O), respectively. These interactions orient the phosphorylamine moiety of Remdesevir toward the Cys145 for the subsequent nucleophilic attack.

Nelfinavir was well fitted into the S1-subsite active pocket of 3CLpro, in which the benzamide carbonyl group and octahydro-*1H*-isoquinoline moiety interact with Gly143 through H-bond and Glu166 by forming H-bond and salt bridge interaction (Figure 9c). Moreover, the phenylsulphanyl group of Nelfinavir stabilized deep into the S2-subsite through hydrophobic π-π interaction with His41. Similarly, to the former compound, the benzamide group positioned toward the Cys145 which susceptible the hydrolytic reaction.

Compound Merimepodib, deposit at the surface of S1-subsite through H-bond interaction with Thr26 (C=O) (Figure 9d). By orienting deeply toward the S4-subsite with the phenyl oxazole moiety, the urido moiety located over the surface of S2-subsite in front of His41-Cys145 dyad, which is critical for inhibiting the catalytic activity of the enzyme.

Taribavirine, which is the nucleoside analogue of ribofuranose mainly, pointed deeply into the S1-subsite (Figure 9e). The 2-hydroxyfuranose and 1, 2, 4-triazole-3-carboximidamide moiety formed H-bond interaction with His164 and the

Preprints (www.preprints.org) | NOT PEER-REVIEWED | Posted: 7 April 2020 doi:10.20944/preprints202004.0084.v1

backbone of Phe140 and Leu14, respectively. Additionally, the last mentioned group formed salt-bridge interaction with Glu166 side chain.

The carbonyl and amino group of 2-amino-3-methylbutanoate moiety of Valaganciclovir stabilizes into the S1 and S4-subsites through H-bond formation with the backbone of Glu166 and Gln189, respectively (Figure 9f). Additionally, the guanine deeply pointed toward the S2-subsite through two H-bond interactions with His41 residue.

As indicated, all of these compounds have the ester moiety or the related bioisoester group like; amide, carboximidamide, uridyl, phosphorylamide and thiophosphate moiety, which stabilized by various type of interactions specially H-bond and hydrophobic with His41 as result, faced them toward the Cys145 which acts as nucleophile.

Figure 10 depicts the binding interaction of the proposed compounds over PLpro active site. Inarigivir posed by U-shape conformation mainly to the S4-subsite (Figure 10a). The adenine moiety formed H-bond interaction with Gln1014, Tyr1009 and interacted through π-π stacking interaction with Tyr1013. In addition, the 2-hydroxyribose group interacted with Arg911 and Asp909 through H-bonding. Furthermore, the thio uridyly group formed H-bond and salt-bridge interaction with Tyr1013 and Arg911, respectively.

Remdesivir expanded over the surface of S2 and S4-subsite. The adenine group oriented toward the S4-subsite (Figure 10b). The phenoxyphosphory amino moiety pointed toward the bottom part of S2-subsite through H-bond interaction with Asp909 and Arg911, while the propionate group twisted to the top of the S2-subsite through H-bond interaction with the backbone of Gln1014.

Preprints (www.preprints.org) | NOT PEER-REVIEWED | Posted: 7 April 2020 doi:10.20944/preprints202004.0084.v1

Nelfinavir was well located into the S4-subsite active pocket of PLpro, in which the benzamide and phenylsulphanyl ring stabilized through T-shape π-π stacking interaction with the side chain of Tyr1013, while the octahydro-1H-isoquinoline moiety oriented to the solvent accessible area of the active site (Figure 10c).

Similarly, Merimepodib is stabilized over S4 and S2-subsite of the active pocket by H-bond formation with key residues Asp909 and Gln1014 and T-shape π-π stacking interaction with Tyr1013 (Figure 10d).

In the case of Taribavirin, the carboximidamide and 1,2,4-triazole groups formed π-cation and T-shape π-π stacking interactions with Tyr1013 and Tyr1009, respectively (Figure 10e). Moreover, with the aid of hydroxyl ribose moiety the compound stabilized at the S4-subsite through H-bond interaction with Asp1047, Ala991 and Tyr1018 residues. Similar to the above mentioned compounds, Valaganciclovir stabilized over the S4-subsite through H-bonding with Asp909, Tyr1018 and Gln1014 as well as salt-bridge interaction with Asp909 (Figure 10f).

Based on investigating the interaction results over PLpro, all the proposed dual inhibitors bind to S2, S4 or both subsites but not to the catalytic site of the PLpro enzyme (His1017, Asp1031 and Cys856). This finding proposed the ability of the mentioned compounds in blocking the entrance of the PLpro active site which appears to prevent substrate access to the catalytic site and inhibiting PLpro enzyme activity.

Among the compounds with proposed dual inhibition feature, Remdesivir (binding energy of -62.96 and -46.23 kcal/mol over 3CLpro and PLpro, respectively) and Inarigrivir (binding energy of -51.21 and -45.15 kcal/mol over 3CLpro and PLpro, respectively) have considerable affinity for both proteases active site. Therefore, more investigation regarding this capability is recommended for these two adenosine

 doi:10.20944/preprints202004.0084.v1

analogue compound. Antiviral activity of Inarigrivir in combination with Tenofovir (an inhibitor of viral polymerase and anti-HIV agent) is already under clinical investigation for Chronic Hepatitis B infection in adults. In 2016, Remdesivir (GS-5734) known as a nucleoside analog is used for as a potential treatment for Ebola (35). Additionally, in 2017, its activity against the coronavirus family (SARS-CoV and MERS-CoV) of viruses was also demonstrated (36, 37). Recently, it being researched as a potential treatment to SARS-CoV2 infection (38).

4. Conclusion

In order to discover repurpose antiviral for dual inhibition of the COVID-19 replication a set exhaustive docking technique were performed through a database of 160 antiviral agents over both 3CLpro and PLpro active sites of SARS-CoV-2. Compounds binding mode and energy were analyzed and ranked. Accordingly, seven antiviral agents including Nelfinavir, Valaganciclovir Merimepodib, Inarigivir, Remdesivir, Taribavirine and TAS106-106 are proposed as potential dual inhibitors of the proteases enzymes necessary for RNA replication. The interatomic result shows the proposed compound located in the 3CLpro active site in a manner that their ester or its bioisoerter faced toward the Cys145, which known as key catalytic residue for hydrolysis through nucleophilic attack (39). In addition, the results reveals the ability of the mentioned compounds in blocking the entrance of the PLpro active site and inhibiting PLpro enzyme activity. More investigation regarding the capability of the extracted compounds is highly recommended.

Acknowledgement

We thank respiratory therapists around the world for the patience, professionalism, hard work, sacrifice, and commitment to providing excellent patient care during the

COVID-19 pandemic. This research did not receive any specific grant from funding agencies in the public, commercial, or not-for-profit sectors

Declaration of Competing Interest

The authors declare that there are no conflicts of interest.

References

1. Summary of probable SARS cases with onsetof illness from 1 November 2002 to 31 July 2003. Communicable Disease Surveillance & Response (CSR); 2004.

2. Pillaiyar T, Manickam M, Jung S. Middle East respiratory syndrome-coronavirus (MERS-CoV): an updated overview and pharmacotherapeutics. Med chem. 2015;5(8):361-72.

3. Li H. China guidelines point to HIV protease inhibitors as potential coronavirus treatment. Biocentury. 2020.

4. Wang M, Cao R, Zhang L, Yang X, Liu J, Xu M, et al. Remdesivir and chloroquine effectively inhibit the recently emerged novel coronavirus (2019-nCoV) in vitro. Cell research. 2020;30(3):269-71.

5. Lu R, Zhao X, Li J, Niu P, Yang B, Wu H, et al. Genomic characterisation and epidemiology of 2019 novel coronavirus: implications for virus origins and receptor binding. The Lancet. 2020;395(10224):565-74.

6. Chen Y, Liu Q, Guo D. Emerging coronaviruses: genome structure, replication, and pathogenesis. Journal of medical virology. 2020.

7. Jin Z, Du X, Xu Y, Deng Y, Liu M, Zhao Y, et al. Structure of Mpro from COVID-19 virus and discovery of its inhibitors. bioRxiv. 2020.

8. Lee T-W, Cherney MM, Huitema C, Liu J, James KE, Powers JC, et al. Crystal structures of the main peptidase from the SARS coronavirus inhibited by a substrate-like aza-peptide epoxide. Journal of molecular biology. 2005;353(5):1137-51.

 doi:10.20944/preprints202004.0084.v1

9. de Wit E, van Doremalen N, Falzarano D, Munster VJ. SARS and MERS: recent insights into emerging coronaviruses. Nature Reviews Microbiology. 2016;14(8):523.

10. Anand K, Ziebuhr J, Wadhwani P, Mesters JR, Hilgenfeld R. Coronavirus main proteinase (3CLpro) structure: basis for design of anti-SARS drugs. Science. 2003;300(5626):1763-7.

11. Hsu M-F, Kuo C-J, Chang K-T, Chang H-C, Chou C-C, Ko T-P, et al. Mechanism of the maturation process of SARS-CoV 3CL protease. Journal of Biological Chemistry. 2005;280(35):31257-66.

12. Báez-Santos YM, John SES, Mesecar AD. The SARS-coronavirus papain-like protease: structure, function and inhibition by designed antiviral compounds. Antiviral research. 2015;115:21-38.

13. Barretto N, Jukneliene D, Ratia K, Chen Z, Mesecar AD, Baker SC. The papain-like protease of severe acute respiratory syndrome coronavirus has deubiquitinating activity. Journal of virology. 2005;79(24):15189-98.

14. Pillaiyar T, Manickam M, Namasivayam V, Hayashi Y, Jung S-H. An Overview of Severe Acute Respiratory Syndrome–Coronavirus (SARS-CoV) 3CL Protease Inhibitors: Peptidomimetics and Small Molecule Chemotherapy. Journal of medicinal chemistry. 2016;59(14):6595-628.

15. Wishart DS, Feunang YD, Guo AC, Lo EJ, Marcu A, Grant JR, et al. DrugBank 5.0: a major update to the DrugBank database for 2018. Nucleic acids research. 2018;46(D1):D1074-D82.

16. Waterhouse A, Bertoni M, Bienert S, Studer G, Tauriello G, Gumienny R, et al. SWISS-MODEL: homology modelling of protein structures and complexes. Nucleic acids research. 2018;46(W1):W296-W303.

17. Schrödinger Suite 2018, Induced Fit Docking protocol; Glide version 5.5, S., LLC, New York, NY, 2009; Prime version 2.1, Schrödinger, LLC, New York, NY, 2009.

18. Schrödinger Release 2018-4: Schrödinger Release 2018-4 Protein Preparation Wizard; Epik, Schrödinger, LLC, New York, NY, 2016; Impact, Schrödinger, LLC, New York, NY, 2016; Prime, Schrödinger, LLC, New York, NY, 2019.

19. Mukherjee P, Desai P, Ross L, White EL, Avery MA. Structure-based virtual screening against SARS-3CLpro to identify novel non-peptidic hits. Bioorganic & medicinal chemistry. 2008;16(7):4138-49.

20. Lee H, Mittal A, Patel K, Gatuz JL, Truong L, Torres J, et al. Identification of novel drug scaffolds for inhibition of SARS-CoV 3-Chymotrypsin-like protease using virtual and high-throughput screenings. Bioorganic & medicinal chemistry. 2014;22(1):167-77.

21. Turlington M, Chun A, Tomar S, Eggler A, Grum-Tokars V, Jacobs J, et al. Discovery of N-(benzo [1, 2, 3] triazol-1-yl)-N-(benzyl) acetamido) phenyl) carboxamides as severe acute respiratory syndrome coronavirus (SARS-CoV) 3CLpro inhibitors: identification of ML300 and noncovalent nanomolar inhibitors with an induced-fit binding. Bioorganic & medicinal chemistry letters. 2013;23(22):6172-7.

22. Schrödinger Release 2018-4: LigPrep, Schrödinger, LLC, New York, NY, 2018.

23. Virtual Screening Workflow 2015-2, Glide version 6.6, LigPrep version 3.3, QikProp version 4.3, Schrödinger, LLC, New York, NY, 2015.

24. Schrödinger Release 2018-4: Prime; MM-GBSA , Schrödinger, LLC, New York, NY, 2018.

25. Benkert P, Biasini M, Schwede T. Toward the estimation of the absolute quality of individual protein structure models. Bioinformatics. 2011;27(3):343-50.

26. Arya R, Das A, Prashar V, Kumar M. Potential inhibitors against papain-like protease of novel coronavirus (SARS-CoV-2) from FDA approved drugs. 2020.

27. Li C, Teng X, Qi Y, Tang B, Shi H, Ma X, et al. Conformational Flexibility of a Short Loop near the Active Site of the SARS-3CLpro is Essential to Maintain Catalytic Activity. Scientific reports. 2016;6:20918.

28. Kong L, Shaw N, Yan L, Lou Z, Rao Z. Structural view and substrate specificity of papain-like protease from avian infectious bronchitis virus. Journal of Biological Chemistry. 2015;290(11):7160-8.

29. Báez-Santos YM, Mielech AM, Deng X, Baker S, Mesecar AD. Catalytic function and substrate specificity of the papain-like protease domain of nsp3 from the Middle East respiratory syndrome coronavirus. Journal of virology. 2014;88(21):12511-27.

30. Erickson JA, Jalaie M, Robertson DH, Lewis RA, Vieth M. Lessons in molecular recognition: the effects of ligand and protein flexibility on molecular docking accuracy. Journal of medicinal chemistry. 2004;47(1):45-55.

31. Nissink JWM, Murray C, Hartshorn M, Verdonk ML, Cole JC, Taylor R. A new test set for validating predictions of protein–ligand interaction. Proteins: Structure, Function, and Bioinformatics. 2002;49(4):457-71.

32. Agostini ML, Andres EL, Sims AC, Graham RL, Sheahan TP, Lu X, et al. Coronavirus susceptibility to the antiviral remdesivir (GS-5734) is mediated by the viral polymerase and the proofreading exoribonuclease. MBio. 2018;9(2):e00221-18.

33. Yao TT, Qian JD, Zhu WY, Wang Y, Wang GQ. A Systematic Review of Lopinavir Therapy for SARS Coronavirus and MERS Coronavirus–A Possible Reference for Coronavirus Disease-19 Treatment Option. Journal of Medical Virology. 2020.

34. Chhikara BS, Rathi B, Singh J, Poonam F. Corona virus SARS-CoV-2 disease COVID-19: Infection, prevention and clinical advances of the prospective chemical drug therapeutics. Chemical Biology Letters. 2020;7(1):63-72.

35. Warren TK, Jordan R, Lo MK, Ray AS, Mackman RL, Soloveva V, et al. Therapeutic efficacy of the small molecule GS-5734 against Ebola virus in rhesus monkeys. Nature. 2016;531(7594):381-5.

36. Sheahan TP, Sims AC, Graham RL, Menachery VD, Gralinski LE, Case JB, et al. Broad-spectrum antiviral GS-5734 inhibits both epidemic and zoonotic coronaviruses. Science translational medicine. 2017;9(396).

37. de Wit E, Feldmann F, Cronin J, Jordan R, Okumura A, Thomas T, et al. Prophylactic and therapeutic remdesivir (GS-5734) treatment in the rhesus macaque model of MERS-CoV infection. Proceedings of the National Academy of Sciences. 2020;117(12):6771-6.

38. Ko W-C, Rolain J-M, Lee N-Y, Chen P-L, Huang C-T, Lee P-I, et al. Arguments in favor of remdesivir for treating SARS-CoV-2 infections. International journal of antimicrobial agents. 2020:105933.

39. Linlin Zhang, Daizong Lin, Xinyuanyuan Sun, Ute Curth, Christian Drosten, Lucie Sauerhering, Stephan Becker, Katharina Rox, Rolf Hilgenfeld. Crystal structure of SARS-CoV-2 main protease provides a basis for design of improved α-ketoamide inhibitors. Science doi:10.1126/science.abb3405 (2020).

 doi:10.20944/preprints202004.0084.v1

Legend of Tables:

Table 1. Binding energy calculation and the type of proposed compound interactions over 3CLpro active site

Table 2. Proposed potential 3CLpro inhibitors (No. 1-21), PLpro (No. 15-34) and the corresponding dual inhibitor (No.15-21), mechanism of action and therapeutic indication. The information are derived from drug bank (https://www.Drugbank.ca)

Table 3. Binding energy calculation and the type of proposed compound interactions over PLpro active site

Preprints (www.preprints.org) | NOT PEER-REVIEWED | Posted: 7 April 2020 doi:10.20944/preprints202004.0084.v1

Table 1. Binding energy calculation and the type of proposed compound interactions over 3CLpro active site

No.	Compound	MMGBSA (Kcal/mol)	Glide score	Interaction over 3CLpro		
				H-Bond	Hydrophobic	Electrostatic
1	**Inarigivir**	-62.96	-6.86	Thr26-His41- Gly143- Ser144-Cys145-Gln189	-	-
2	**Telaprevir**	-62.70	-7.28	Ser46-Glu166-Gln189	-	-
3	**Indinavir**	-55.97	-7.23	Gly43-Asn142	His41	Glu166
4	**Adafosbuvir**	-55.02	-6.20	Gly143-Gly170-Gln189	His41	-
5	**Tenofovir**	-51.48	-6.40	Thr26- Glu166-Gln189	His41	-
6	**Remdesivir**	-51.21	-6.58	His41- Cys44- Gly143-Glu166- Thr190	His41	-
7	**Valaganciclovir**	-50.93	-7.29	Asn142-Glu166-Gln189	-	-
8	**Amprenavir**	-50.32	-8.62	Thr45- Asn142- Glu166-Gln189-Thr190	-	-
9	**Boceprevir**	-48.68	-7.56	Thr26- Asn142- Glu166-Gln189	-	-
10	**Merimepodib**	-46.97	-6.18	Thr26-Asn119	-	-
11	**Sofosbuvir**	-46.51	-6.16	Thr45- Asn142-Glu166	-	-
12	**Asunaprevir**	-46.46	-6.14	Asn142	-	-
13	**L-756423**	-45.92	-7.30	His41-Asn142-Glu166	His41-His172	Glu166
14	**Darunavir**	-43.08	-6.21	-	His41	-
15	**Atazanavir**	-42.45	-6.91	Asn142- Glu166-Gln189	His41	-
16	**Nelfinavir**	-41.86	-6.50	Asn142	His41	Glu166
17	**Taribavirin**	-40.17	-6.24	Phe140-Leu141-His164- Glu166-Leu167	-	Glu166
18	**TAS-106**	-38.95	-7.25	Leu141-His164- Met165-Glu166	-	-
19	**Galidesivir**	-35.19	-6.34	His41-Glu166-Leu167-Gln189	-	-
20	**ZZ2-PJ**	-33.31	-6.10	Asn142	-	-
21	**Sorivudine**	-30.39	-6.57	Glu166-Gln189	His41-Thr190	-
22	**Ritonavir**	-25.49	-7.14	Asn142-Glu160-Gln189	His41	-

Preprints (www.preprints.org) | NOT PEER-REVIEWED | Posted: 7 April 2020 doi:10.20944/preprints202004.0084.v1

Table 2: Proposed potential 3CLpro inhibitors (No. 1-21), PLpro (No. 15-34) and the corresponding dual inhibitor (No.15-21), mechanism of action and therapeutic indication. The information are derived from drug bank (https://www.Drugbank.ca)

No	Name (DB No.[1])	Group	Mechanism of Action	Indication/ Organism
1	Adafosbuvir (DB14906)	Investigational	NA	Chronic Hepatitis C Virus (HCV) Infection/HCV
2	Amprenavir (DB00701)	Approved/ Investigational	Inhibitor of HIV viral proteinase enzyme	HIV-1 infection/HIV
3	Asunaprevir (DB11586)	Approved	Inhibitor of HCV NS3 protease	Chronic hepatitis C/HCV
4	Atazanavir (DB01072)	Approved/ Investigational	Inhibitor of HIV-1 protease	HIV-1 infection/HIV
5	Boceprevir (DB08873)	Approved/ Investigational	Inhibitor of NS3/4A serine protease enzyme	Chronic HCV genotype 1 infection/HCV
6	Darunavir (DB01264)	Approved	Inhibitor of HIV protease	Human immunodeficiency virus (HIV) infection/HIV, SARS-CoV-2
7	Galidesivir (DB11676)	Investigational	Inhibitor of viral RNA polymerase	Has been investigated for use against Zaire Ebolavirus. It may be studied as a potential therapy for COVID-19/ Zaire Ebolavirus, SARS-CoV-2
8	Indinavir (DB00224)	Approved	Inhibitor of HIV viral protease enzyme	HIV infection/HIV
9	L-756423 (DB02009)	Experimental	Inhibitor of P-glycoprotein I (Predicted feature)	NA
10	Ritonavir (DB00503)	Approved/ Investigational	Inhibitor of HIV-1 protease	HIV-1 infection/HIV, SARS-CoV-2
11	Sofosbuvir (DB08934)	Approved	Inhibitor of HCV NS5B (non-structural protein 5B) RNA-dependent RNA polymerase	HCV and HIV co-infected patients/HCV, HIV
12	Sorivudine (DB11998)	Investigational	NA	Chickenpox and HIV Infections/NA
13	Telaprevir (DB05521)	Approved/ Withdrawn	Inhibitor of NS3/4A serine protease enzyme	Chronic HCV genotype 1 infection/HCV
14	Tenofovir-Alafenamide (DB09299)	Approved	Inhibitor of viral polymerase	Chronic hepatitis B For the treatment of HIV-1 infection/HIV
15	Inarigivir (DB11586)	Investigational	NA[2]	Chronic Hepatitis B/NA

Preprints (www.preprints.org) | NOT PEER-REVIEWED | Posted: 7 April 2020 doi:10.20944/preprints202004.0084.v1

16	Merimepodib (DB04862)	Investigational	Inhibitor of inosine monophospate dehydrogenase (IMPDH)	Hepatitis C virus (HCV) infection/HCV and other RNA/DNA viruses
17	Nelfinavir (DB00220)	Approved	Inhibitor of the HIV viral proteinase enzyme	HIV-1 infection/HIV
18	Remdesivir (DB14761)	Investigational	Inhibitor of RNA polymerase	Variety of RNA viruses/ Coronavirus (CoV) family of viruses, such as SARS-CoV and MERS-CoV
19	Taribavirin (DB06408)	Investigational	Inhibitor of inosine monophosphate (IMP) dehydrogenase	hepatitis (viral, C) infection/NA
20	TAS-106 (DB06656)	Investigational	Inhibitor of of RNA polymerases I, II and III	Investigated for use/treatment in solid tumors and cancer/tumors (unspecified)/NA
21	Valganciclovir (DB01610)	Approved/ Investigational	Inhibitor of viral DNA polymerases	Cytomegalovirus infections/ Herpes Virus
22	Ascorbic acid (DB 00126)	Approved/ Nutraceutical	Involved in synthesis of lipids and proteins, resistance to infections, and cellular respiration.	**H**as been suggested to be an effective antiviral agent/ NA
23	Cytarabine (DB00987)	Approved /Investigational	Inhibitor of DNA polymerase	**B**eing investigated for its antiviral properties/ NA
24	2-deoxyglucose (DB08831)	Experimental/ Investigational	Inhibitor of glycolysis	Herpes simplex infection/ NA
25	Elsulfavirine (DB14929) *****	Investigational	NA[2]	Hepatic Impairment/ NA
26	Faldaprevir (DB11808)	Investigational	NA	Chronic Hepatitis C/ NA
26	Famciclovir (DB00426)	Approved /Investigational	Inhibitor of HSV-2 DNA polymerase	Acute herpes zoster and suppression of recurrent genital herpes/ HHV
27	GS-6620 (DB15222)	Investigational	NA	Chronic Hepatitis C Virus Infection/ NA
28	5-Guanylylmethylene bisphosphonate (DB03725)	Experimental	NA	NA/NA
29	Penciclovir (DB00299)	Approved	**I**nhibitor of viral DNA polymerase	Recurrent cold sores on the lips and face from various herpesvirus infections/ HSV
30	Lopinavir (DB01601)	Approved /Investigational	**I**nhibitor of the HIV-1 protease enzyme	HIV-1 infection/ HIV, **S**ARS-CoV-2
31	Maribavir	Investigational	Inhibitor oh inhibit viral DNA assembly	Under Investigation for use/treatment in viral infection and cytomegalovirus (CMV) retinitis
32	Ribavirin (DB00811)	Approved	Virus mutagen, **I**nhibitor of host inosine monophosphate dehydrogenase,	Chronic Hepatitis C virus (HCV) infection and Severe Respiratory Syncytial Virus Infection/ HBV, HCV,RSV

Preprints (www.preprints.org) | NOT PEER-REVIEWED | Posted: 7 April 2020 doi:10.20944/preprints202004.0084.v1

			Direct Inhibitor viral mRNA polymerase	
33	Vidarabine (DB00194)	Approved /Investigational	**I**nhibitor of viral DNA polymerase	chickenpox - varicella, herpes zoster and herpes simplex infection/ HSV
34	Zanamivir (DB00558)	Approved, Investigational	**I**nhibitor of influenza virus neuraminidase	Influenza A and B infection/IAV, IBV[3]

[1]DB no.: Drug Bank Accession Number,[2]NA: Not Available, [3]IAV and IBV: Influenza A virus and Influenza B virus

Preprints (www.preprints.org) | NOT PEER-REVIEWED | Posted: 7 April 2020 doi:10.20944/preprints202004.0084.v1

Table 3. Binding energy calculation and the type of proposed compound interactions over PLpro active site

No.	Compound	MMGBSA (Kcal/mol)	Glid score	Interaction over PLpro		
				H-Bond	Hydrophobic	Electrostatic
1	**Elsulfavirine**	-76.13	-6.970	Lys902-Asp909- Asn1012-Gln1014-Tyr1018	Tyr1013	Lys902
2	**Merimepodib**	-67.51	-7.022	Asp909- Asn1012-Tyr1013-Gln1014	Tyr1013	-
3	**Lopinavir**	-61.53	-6.251	Arg911	Tyr1013	-
4	**Maribavir**	-53.75	-6.810	Asp909- Gln1014-Tyr1018	Tyr1013	-
5	**Faldaprevir**	-50.77	-6.650	Asp909-Arg911-Glu912-Tyr1013	-	-
6	**Famciclovir**	-47.28	-6.266	-	Tyr1013	-
7	**Inarigivir**	-46.23	-6.400	Asp909-Arg911-Tyr1009-Tyr1013-Gln1014	Tyr1013	Arg911
8	**Remdesivir**	-45.15	-8.015	Asp909-Arg911	-	-
9	**GS-6620**	-44.73	-6.94	Asp909-Arg911- Tyr1013-Gln1014	-	-
10	**Nelfinavir**	-43.48	-6.69	Glu912-Gln1014	Tyr1013	Glu912
11	**Valaganciclovir**	-42.21	-6.29	Asp909-Gln1014-Tyr1018	Tyr1013	-
12	**Penciclovir**	-41.75	-6.23	Asp909-Arg911-Tyr1018	Tyr1013-Tyr1009	
13	**Valganciclovir**	-39.13	-6.30	Asp909- Gly1011- Gln1014-Tyr1018	-	Asp909
14	**Vidarabine**	-38.36	-7.18	Leu907-Asp909-Gln1014	Tyr1013	-
15	**Taribavirin**	-36.33	-6.83	Ala991- Gln1014-Tyr1018-Asp1047	Tyr1009-Tyr1013	-
16	**Cytarabine**	-34.78	-8.32	Leu907-Gln1014	Tyr1013	-
17	**5-Guanylylmethylenebisphosphonate**	-34.20	-6.62	Asp909-Arg911-Tyr1018	Tyr1013-Tyr1009	Asp911
18	**TAS-106**	-27.93	-7.47	Gln1014-Asp1047	-	-
19	**Acorbic-acid**	-25.33	-6.53	Asp909-Arg911-Tyr1018	-	-
20	**2-deoxyglucose**	-25.16	-7.37	Asp909-Ala991-Tyr1013-Tyr1018	-	-
21	**Ribavirin**	-22.55	-6.82	Asp909- Gln1014-Tyr1018-Asp1047	-	-
22	**Zanamivir**	-19.83	-7.37	Asp909-Tyr1018	-	-

Preprints (www.preprints.org) | NOT PEER-REVIEWED | Posted: 7 April 2020 doi:10.20944/preprints202004.0084.v1

Legend of Figures:

Figure 1. Sequence alignment of SARS-CoV-2 and SARS-CoV PLpro catalytic domain (PDB code: 3E9S) generated by CLUSTALW algorithm. An asterisk, a colon, and a full stop represent the conserved residue, conserved substitution, and semi-conserved substitution, respectively.

Figure 2. Local Quality plot of SARS-CoV-2 PLpro model

Figure 3. SARS-CoV-2 PLpro model comparison plot

Figure 4. 3D representation of 3CLpro (a) and PLpro (b) active site. In the case of 3CLpro domain I, domain II and the long loop between domain II and III colored in green, cyan and orange, respectively.

Figure 5. Close-up representation of binding interactions of the superposed docked (cyan) and co-crystalized ligand (green) RZs and TTT over SARS-CoV-2 3CLpro (a) protease (5R82) and PLpro (b), respectively. Structural water and residues responsible for H-bond interaction render are in stick. The hydrogen bonding and π-π stacking interactions are represented as yellow, blue, respectively.

Figure 6. 2D representation of compounds with high binding affinity for 3CLpro active site (except those with dual affinities).

Figure 7. 2D representation of compounds with high binding affinity for both 3CLpro and PLpro active sites.

Figure 8. 2D representation of compounds with high binding affinity for PLpro active site (except those with dual affinities).

Figure 9. 3D binding mode of Inarigivir (a), Remdesivir (b), Nelfinavir (c), Merimepodib (d), Taribavirine (e) and Valagancyclovir (f) over 3CLpro active site. The active compounds are showed as sticks and colored in green. The hydrogen

 doi:10.20944/preprints202004.0084.v1

bonding, π-π stacking, and electrostatic interactions are represented as yellow, blue, and purple dashed lines, respectively. Domain I, domain II and long loop connecting domain II and III colored in light green, cyan and orange, respectively.

Figure 10. 3D binding mode of Inarigivir (a), Remdesivir (b), Nelfinavir (c), Merimepodib (d), Taribavirine (e) and Valagancyclovir (f) over PLpro active site. The active compounds are showed as sticks and colored in green. The hydrogen bonding, π-π stacking, and electrostatic interactions are represented as yellow, blue, and purple dashed lines, respectively.

Preprints (www.preprints.org) | NOT PEER-REVIEWED | Posted: 7 April 2020 doi:10.20944/preprints202004.0084.v1

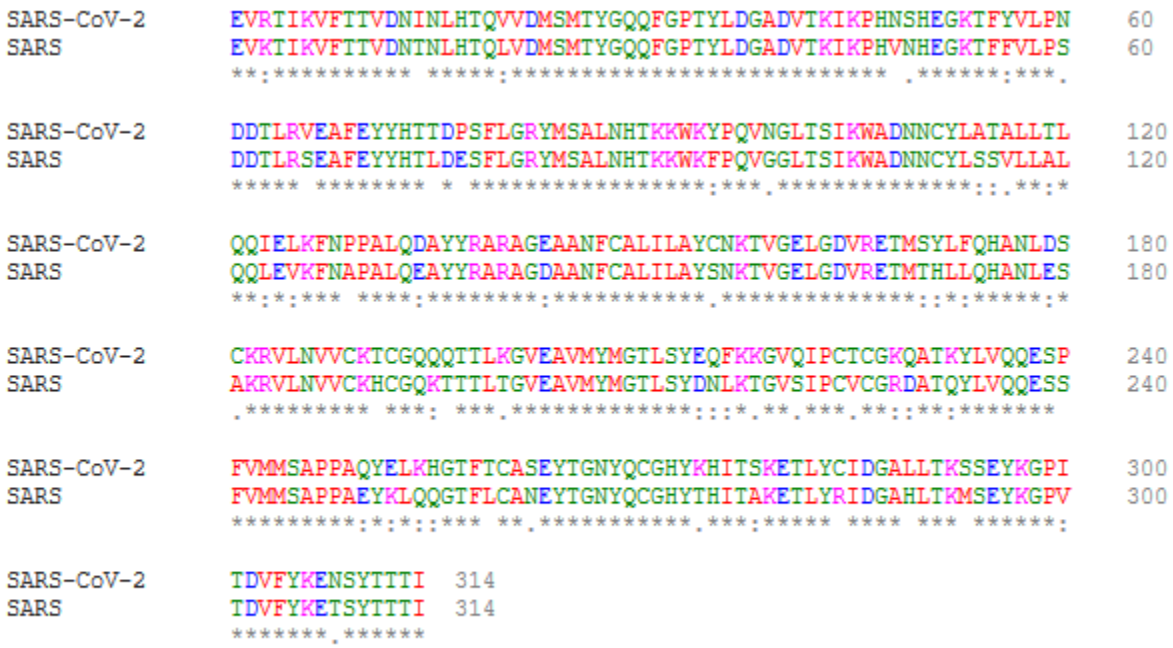

Figure 1

Preprints (www.preprints.org) | NOT PEER-REVIEWED | Posted: 7 April 2020 doi:10.20944/preprints202004.0084.v1

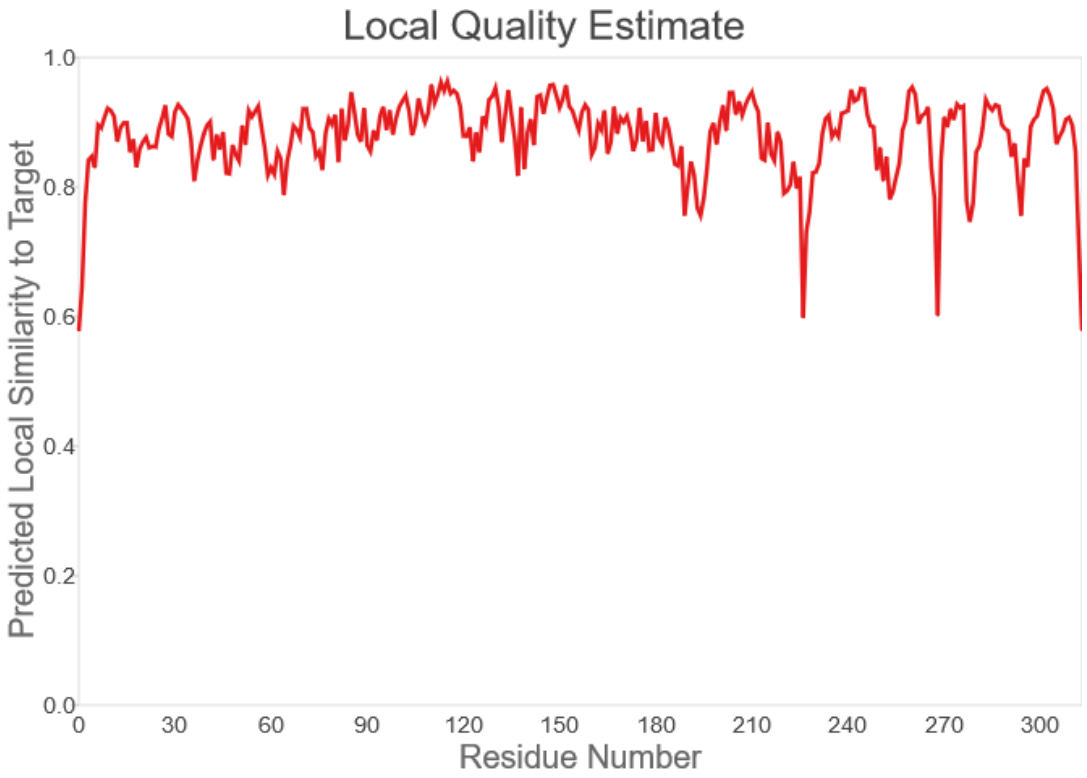

Figure 2

Preprints (www.preprints.org) | NOT PEER-REVIEWED | Posted: 7 April 2020 doi:10.20944/preprints202004.0084.v1

Figure 3

Preprints (www.preprints.org) | NOT PEER-REVIEWED | Posted: 7 April 2020 doi:10.20944/preprints202004.0084.v1

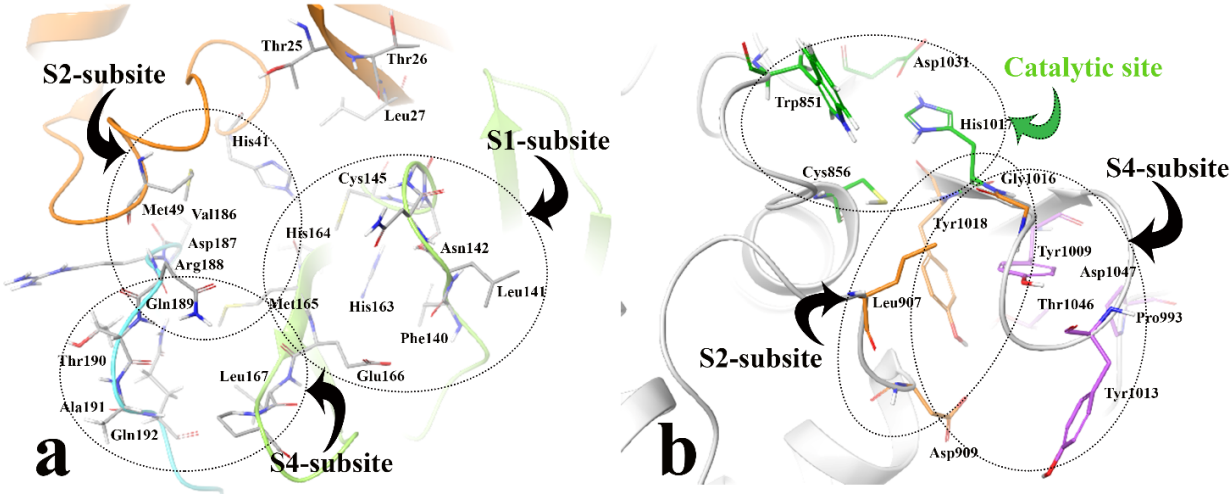

Figure4

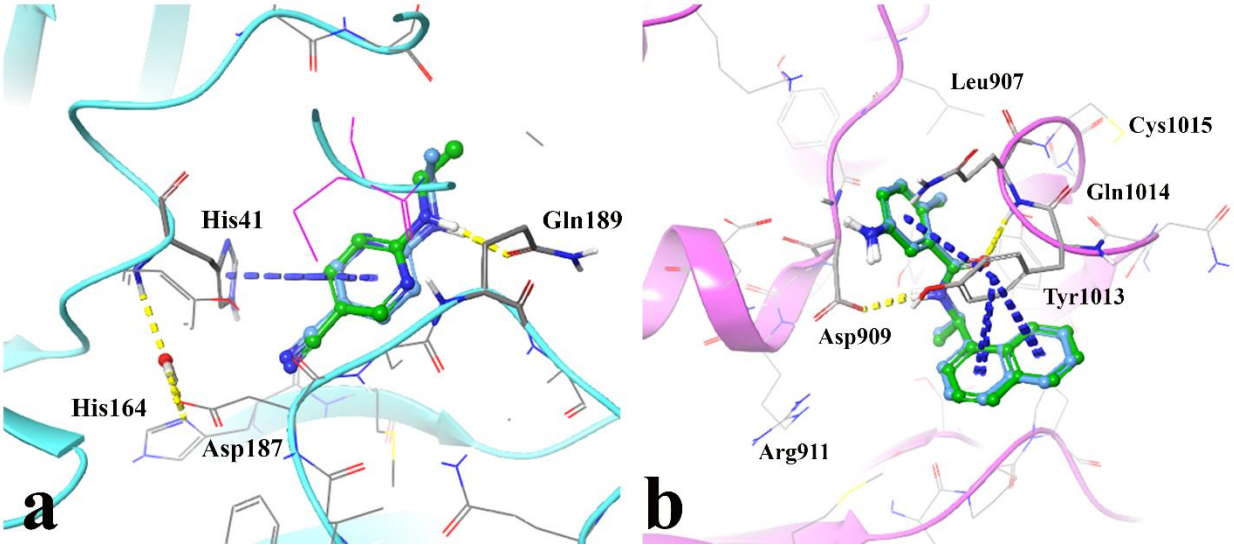

Figure 5

Preprints (www.preprints.org) | NOT PEER-REVIEWED | Posted: 7 April 2020 doi:10.20944/preprints202004.0084.v1

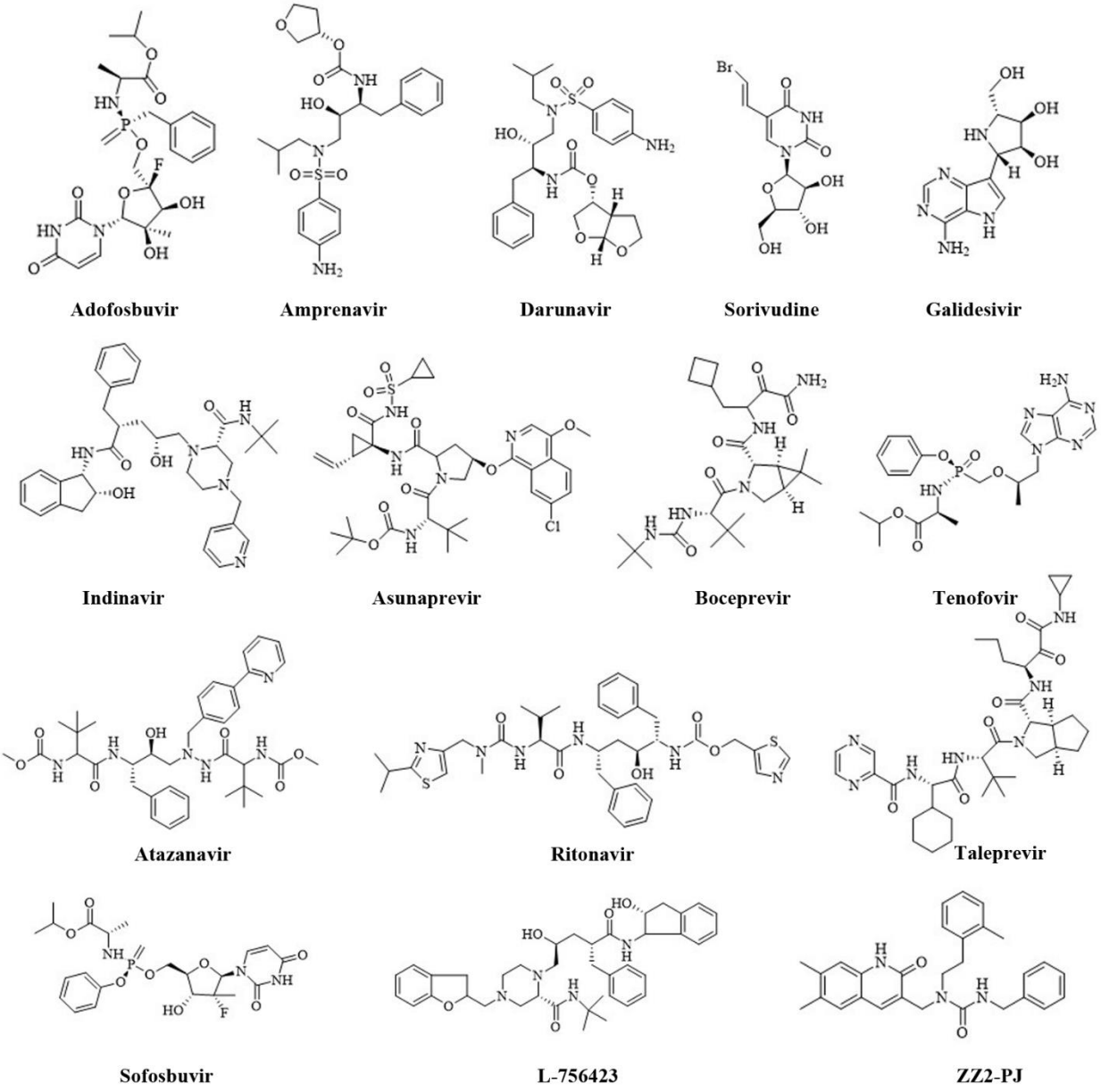

Figure 6

Preprints (www.preprints.org) | NOT PEER-REVIEWED | Posted: 7 April 2020 doi:10.20944/preprints202004.0084.v1

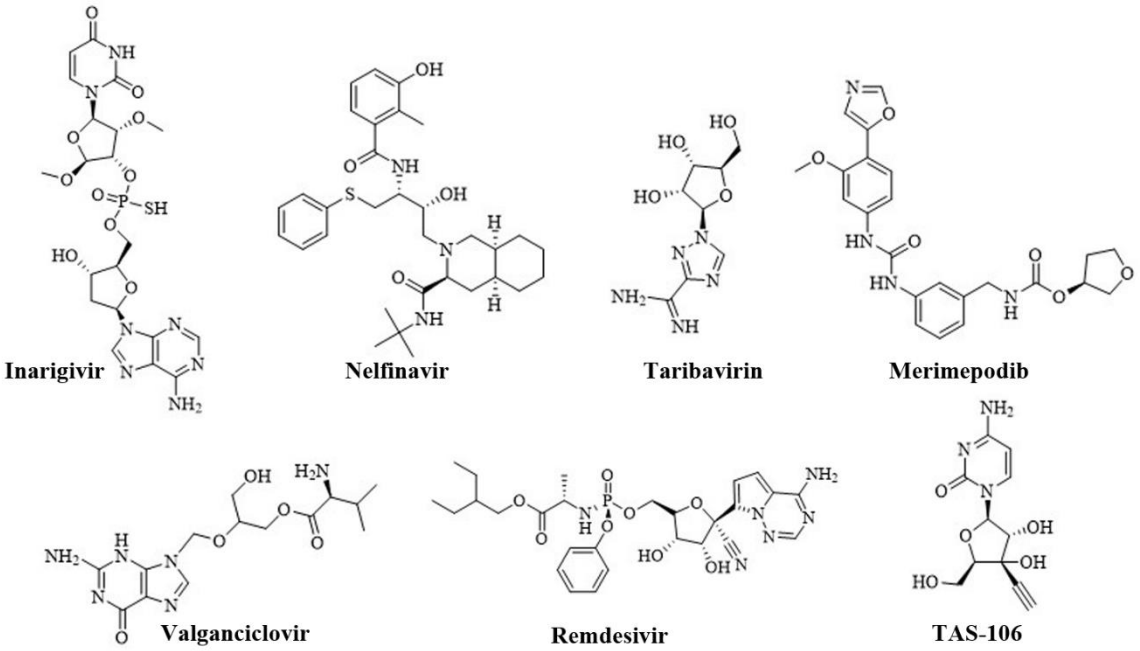

Figure 7

Preprints (www.preprints.org) | NOT PEER-REVIEWED | Posted: 7 April 2020 doi:10.20944/preprints202004.0084.v1

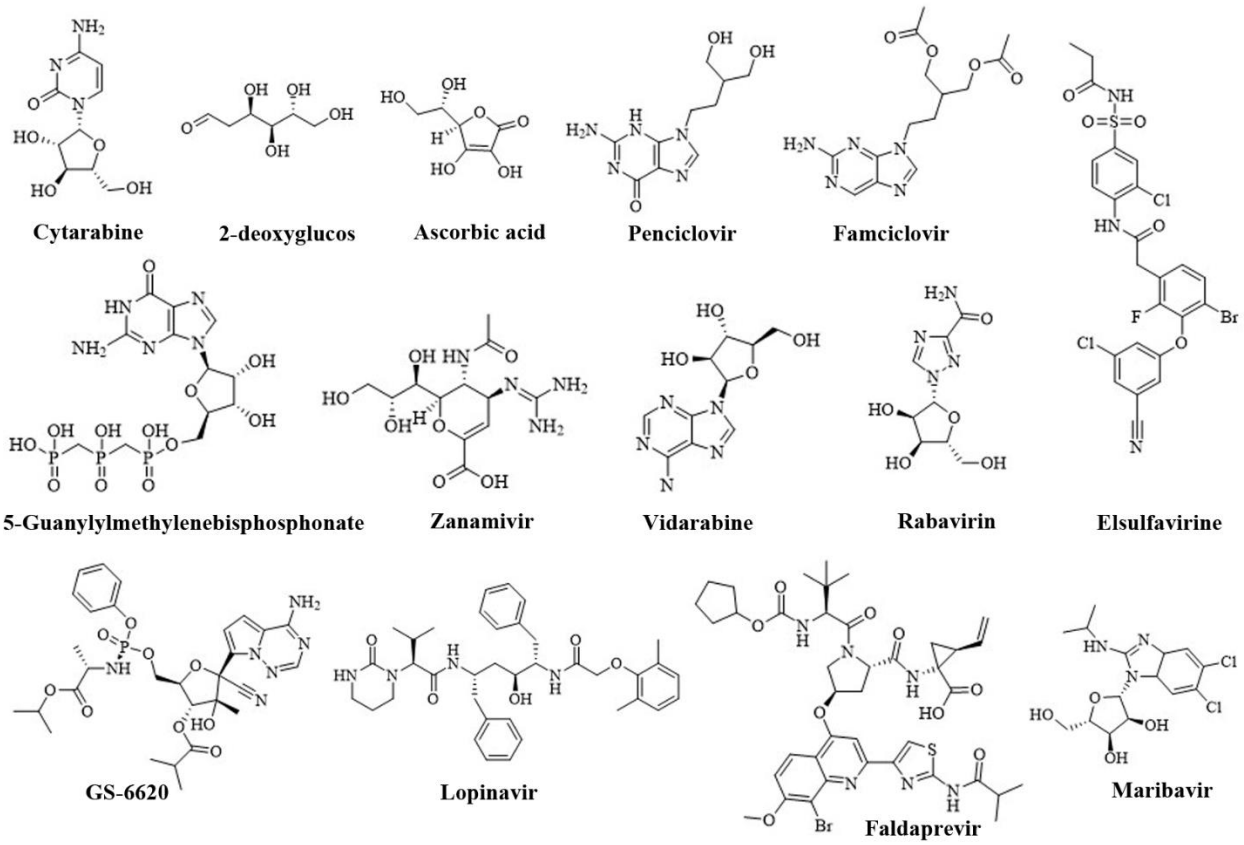

Figure 8

Preprints (www.preprints.org) | NOT PEER-REVIEWED | Posted: 7 April 2020 doi:10.20944/preprints202004.0084.v1

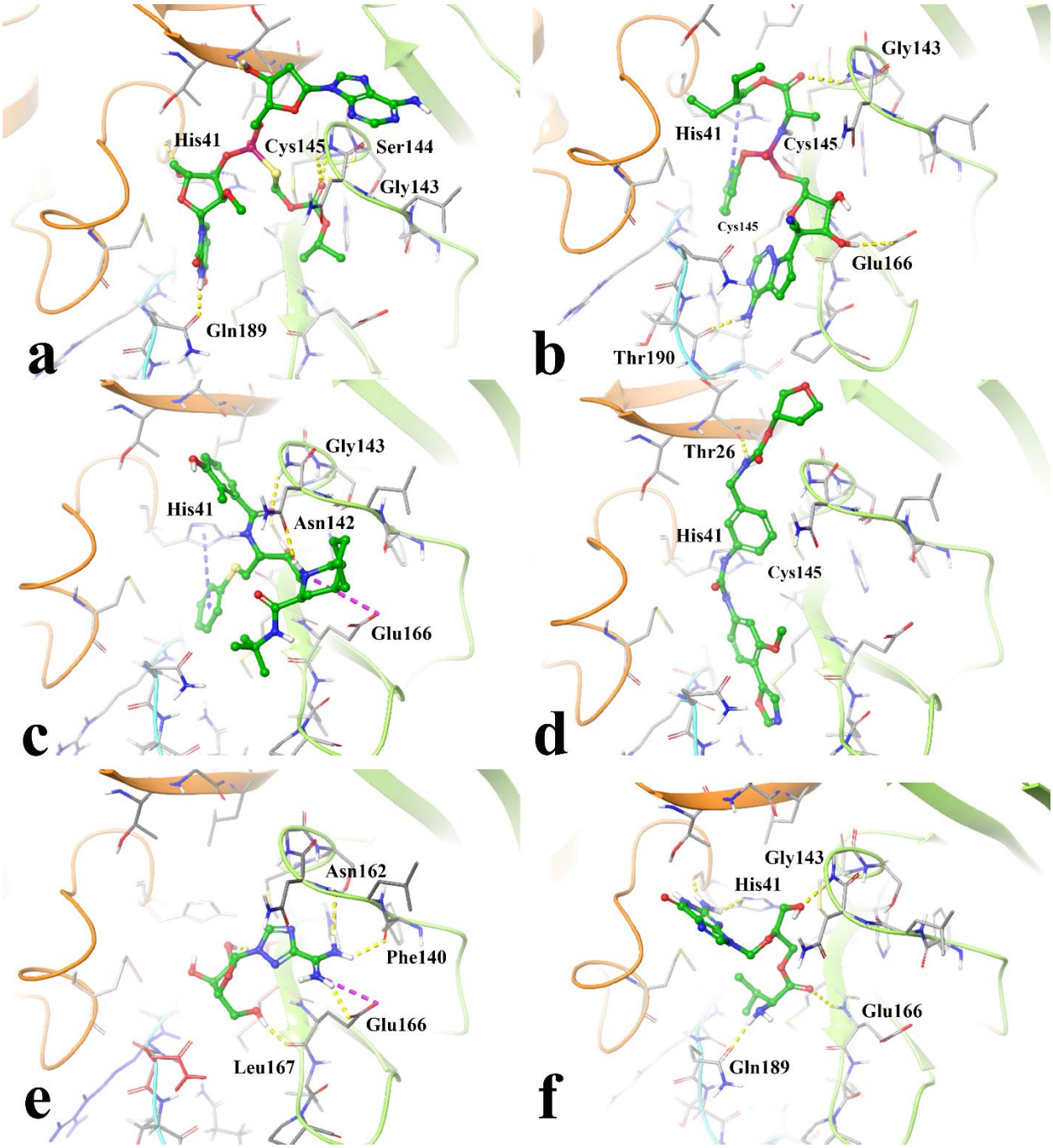

Figure 9

Preprints (www.preprints.org) | NOT PEER-REVIEWED | Posted: 7 April 2020 doi:10.20944/preprints202004.0084.v1

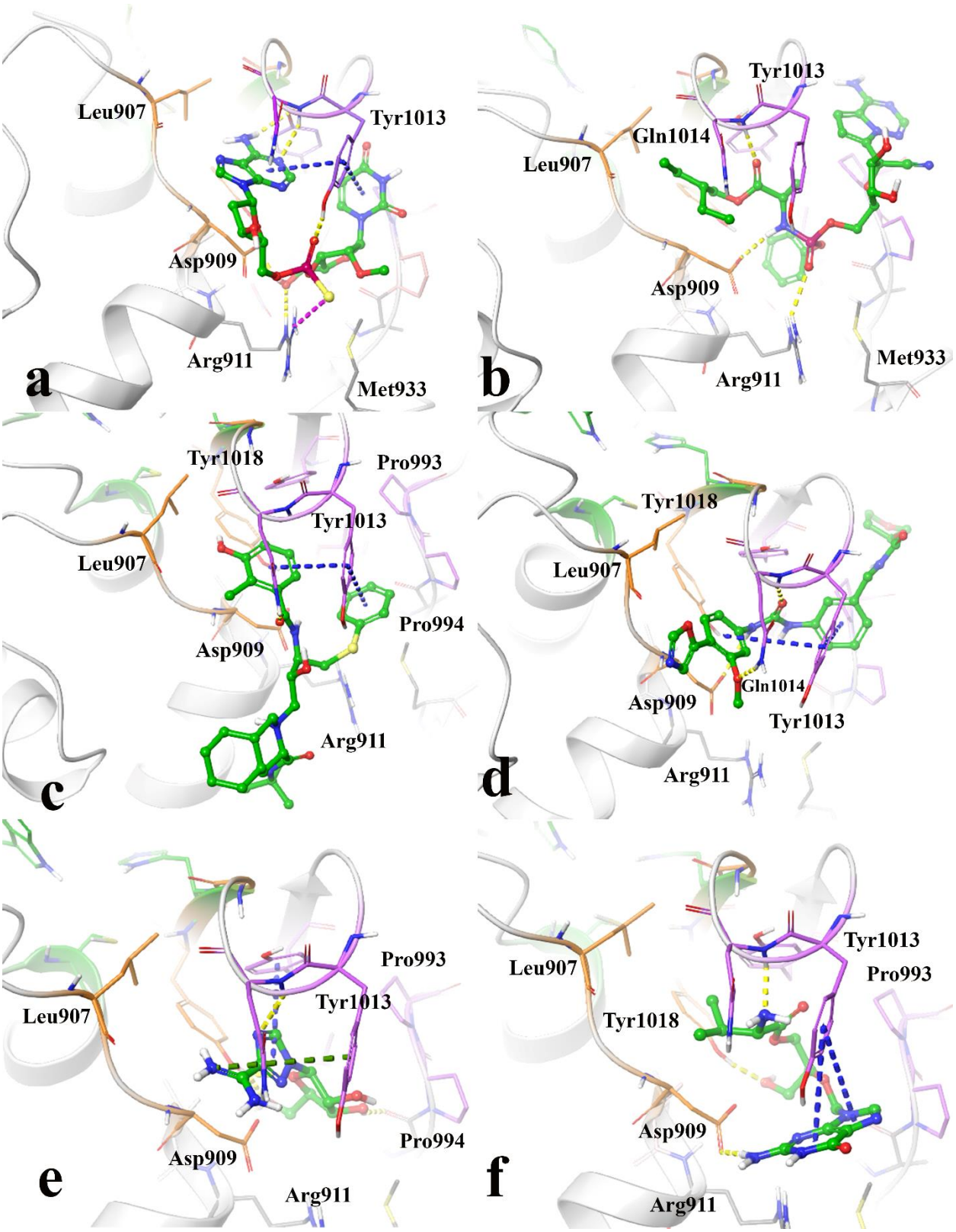

Figure 10